Journal of Materials Chemistry A

Accepted Manuscript

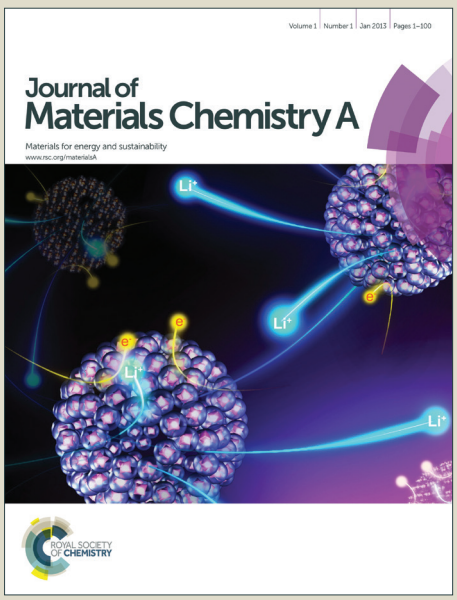

ROYAL SOCIETY OF CHEMISTRY

www.rsc.org/materialsA

Cite this: DOI: 10.1039/c0xx00000x

www.rsc.org/xxxxxx

ARTICLE TYPE

A polymer-metal-polymer-metal heterostructure for enhanced photocatalytic hydrogen production

Yifeng Zhang,[a] Fang Mao[a], Hongjian Yan,*[b] Kewei Liu,[b] Hongmei Cao,[b] Jiagang Wu,[a] Dingquan Xiao*[a]

Received (in XXX, XXX) Xth XXXXXXXXX 20XX, Accepted Xth XXXXXXXXX 20XX

DOI: 10.1039/b000000x

The tightly coupled heterostructure g-C_3N_4/Au/poly(3-hexylthiophene) (P3HT)/Pt was successfully prepared by self-assembling method. The heterojunction photocatalyst displayed high activity for hydrogen production from water which contains triethanolamine as an electron donor under visible light irradiation. The samples were characterized by X-ray diffraction (XRD), UV-vis spectroscopy, photoluminescence (PL) spectra analysis and transmission electron microscopy (TEM), respectively. The experimental results demonstrated that the g-C_3N_4/Au/P3HT/Pt structure was conducive to the efficiently separation of photo-generated electron-hole pairs, which can be explained by the strong junction of chemical bond between Au and P3HT. The effect of P3HT content on the activity of the photocatalysts was investigated with a series of g-C_3N_4/Au/P3HT heterostructure samples loaded Pt as a cocatalyst in triethanolamine aqueous solutions**.** The optimal P3HT content was determined to be 0.5 wt%, and the corresponding hydrogen evolution rate was 320 μmol h^{-1}.

Introduction

Hydrogen is widely regarded as a potential solution to solve the energy and environment issues at global level. The photocatalytic water-splitting plays a vital role in hydrogen production methods for the transition from a carbon-based energy system to a hydrogen-based energy system. The photocatalytic splitting of water, without the electricity, directly conversing sunlight into hydrogen and oxygen, will be the trump card that does not involve carbon oxide emission like the manufacture of hydrogen from fossil fuels or biological reformation of biomass. Obtaining sustainable hydrogen production to supply the amounts required needs the advanced materials, synthetic technologies and the new design concepts. [1, 2]

Since the Fujishima and Honda found the TiO_2 can cleavage water under the ultraviolet light,[3] the metal-based inorganic materials (including the metal-oxides, metal-(oxy)nitride, metal-oxysulfides) occupy the field of photocatalysts with absolute dominance.[4] Although the inorganic materials have made remarkable achievements in this field, the noble or rare elements are the main constituents of the metal-based complexes.[5] Seeking green, sustainable and inexpensive photocatalysts made of abundant elements that we can obtain conveniently on the earth is significant for the utilization of solar energy in practical application. Therefore, organic photocatalysts for artificial photosynthesis has been developed to explore a more economical and environmental friendly manner. Recently, the polymeric organic semiconductor g-C_3N_4 shows the ability of water splitting for hydrogen production under visible light.[6] The utilization of the polymeric organic semiconductors, which are cheap and easily available materials, opens up a new prospect to construct the high efficient and economical photocatalysis system. However, the g-C_3N_4 photocatalysts suffer from many problems, such as the high excitation dissociation energy, low charge mobility, low specific surface area, insufficient visible photons absorption and high level of the top of the valance band.[7] In order to boost the photocatalytic efficiency of g-C_3N_4, several strategies, such as the new synthesis methods,[8-15] doping with metal or non-metal elements,[16,17] dye sensitization,[18,19] surface modification [20-22] and construction of complexes based on g-C_3N_4,[23-30] have been developed. These methods have been proved to be effective for the promotion of the photocatalytic activity of g-C_3N_4.

In our previous work, the physical adsorption of poly(3-hexylthiophene) (P3HT) on the surface of g-C_3N_4 was obtained by evaporation of the solvent using a water bath.[29] However, the g-C_3N_4 with P3HT cannot be intimately combined by the week Van der waals force. This could reduce the photo-generated electrons transfer efficiency between P3HT and g-C_3N_4. Herein, we adopted the chemical bond to ensure the tightly conjunction between g-C_3N_4 and P3HT. Substitute the chemical adsorption for the physical adsorption can solve the separation problem of g-C_3N_4 and P3HT, and therefore we can realize the cyclic utilization of catalysts. The formation of tightly g-C_3N_4/Au heterojunction was obtained by the photodeposition method. In addition, 0.5 wt % Pt was loaded on the P3HT as a co-catalyst to provide chemical reactivity or active site for H_2 evolution, and improve the photocatalytic activity of catalysts.[20] To the best of our knowledge, this is the first time to fabricate the polymer-metal-polymer-metal heterostructure for photocatalytic water splitting.

Experimental section

sample preparation

Melamine, sulfuric acid (H_2SO_4), tetrahydrofuran (THF) and triethanolamine (TEA) were purchased from Chengdu Kelong Chemical Reagent Factory. Pluronic P123 was purchased from Aldrich. The P3HT was bought from Luminescence Technology Corp. All reagents were used as received without further treatment.

Preparation of g-C_3N_4: The g-C_3N_4 was synthesized via soft-templating method by using Pluronic P123 surfactant as soft template.[12] The Pluronic P123 (5.0 g) and melamine (25.0 g) were dispersed in distilled water (500 mL) successively and heated at 100 ^oC for 1 h under magnetic stirring. Then sulfuric acid solution (10 mL, H_2SO_4:H_2O = 1:1 in volume) was slowly added into the solution, and white precipitate was produced. After cooling down to room temperature, the precipitate was collected by filtration. After dried in an oven at 80 □ for over night, the precipitate was heated from room temperature to 380 ^oC in 5 minutes and then to 600 ^oC at a heating rate of 1 ^oC min^{-1} and then maintained at 600 ^oC for 4 hours in a muffle furnace in the flow of Ar gas. After the reaction, the product was cooled down to room temperature in the flow of Ar gas. Finally, the product was then calcined at 500 ^oC for 2 h in air.

The loading of 1 wt% Au on the g-C_3N_4: g-C_3N_4 (1 g) was dispersed in 200 mL 10% (in volume) TEA solution containing a certain amount of $HAuCl_4$ solution. After evacuated the air completely, the mixture was irradiated with Xe lamp (300 W) for 30 minutes at room temperature. After irradiation, the sample was collected by filtration and then dried at 60□ in an oven for overnight.

Preparation of g-C_3N_4/Au/P3HT/Pt: The P3HT/Pt was prepared by photoreduction method. Typically, chloroplatinic acid (0.5 mg), P3HT (0.5 mg) and isopropanol alcohol (0.2 mL) was dissolved in THF (16 mL). The solution was irradiated by Xe lamp (300 W) for 30 minutes at room temperature. Then, 0.1 g g-C_3N_4/Au was added in the solution. The solution was stirred at room temperature for 2 hours in the dark. The slurry was filtrated and washed with THF, acetone and 10% TEA sequentially. Then the photocatalyst was transferred to the reaction cell for potocatalytic reaction test.

Photocatalytic reaction

In a typical photocatalytic experiment, the reaction was performed in a top irradiation-type Pyrex vessel connected to a glass closed gas circulation system. Photoreduction of H^+ to H_2 was conducted in the reaction system with an aqueous TEA solution (TEA, 10 vol %, 200mL) as the sacrificial reagent. The light source was a 300 W xenon lamp fitted with a cutoff filter (λ>420nm). Prior to irradiation, the reactant solution was evacuated to remove dissolved air completely. During the reaction, a flow of cooling water was used to maintain the reactant solution at room temperature. The generated gases were detected by gas chromatography (SPSIC, GC-102AT, argon carrier).

Characterization

X-ray diffraction (XRD) patterns were obtained on a X-Pert Pro diffraction meter with Cu K_α radiation (λ=1.5406 Å) at a scan step size of 0.03^o. UV-vis diffuse reflection spectra were recorded on a UV-vis spectrophotometer (UV3600, Shimadzu) and converted from reflection to absorbance by the Kubelka-Munk method. $BaSO_4$ was used as a reflectance standard in the UV-visible diffuse reflectance experiment. The photoluminescence (PL) measurements were taken with a fluorescence spectrophotometer (Hitachi F-7000) and operated at room temperature. The excitation wavelength was 279 nm. Transmission electron microscopy (TEM) images were conducted on high-resolution transmission electron microscopy (HRTEM; JEM-2010F, JEOL). X-ray photoelectron spectroscopy (XPS) spectra were collected on a V4105 instrument (Thermo Electron, USA) with a Mn Kα radiation source.

Results and discussions

Phase Structures, Morphology and Fine structure

The XRD patterns of g-C_3N_4, g-C_3N_4/Au, and g-C_3N_4/Au/P3HT/Pt nanosheets are shown in Figure 1. All the diffraction curves have the same diffraction peaks at 27.7^o and 12.9^o, corresponding to the interplanar distance of 0.322 nm and 0.682 nm, respectively. The peak at 27.7^o is due to the interlayer stacking peak of aromatic systems, while the peak at 12.9^o is related to the in-planar repeat period (ex.the hole-to-hole distance in the nitride pores).[6,15,31] The results were in good agreement with the previous reports about g-C_3N_4 and indicated that the main phase of g-C_3N_4 in the samples would not be changed by the metal loading or composite process. The diffraction peaks at 38.2° and 44.4° in the XRD patterns (See in Figure 1 b and c) can be indexed to the (111) and (200) planes of Au metal particles. Both the diffraction peaks of g-C_3N_4 and Au appeared in curve b and c, indicating that the Au was loaded on the g-C_3N_4 successfully. However, the diffraction peaks of P3HT and Pt were not detected in the sample of g-C_3N_4/Au/P3HT/Pt, because neither of their amounts was obviously too high to form a separate phase alone.

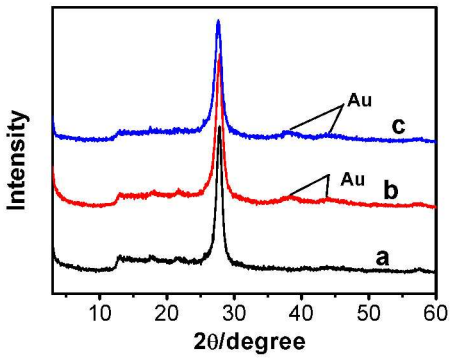

Figure 1 XRD pattern of (a) g-C_3N_4, (b) g-C_3N_4/Au, and (c) g-C_3N_4/Au/P3HT/Pt

TEM was used to study the morphology and microstructures of the g-C_3N_4, g-C_3N_4/Au, P3HT/Pt, and the heterostructure g-C_3N_4/Au/P3HT/Pt, respectively. As shown in Figure 2(a), the g-C_3N_4 has layer structure and is a thin sheet with irregular

morphology. Figure 2(b) shows that the regularly spherical Au nanoparticles with size of 3~5 nm were uniformly loaded on the surface of g-C_3N_4. The Au lattice fringes were distinctly observed as shown in the insert in Figure 2(b). The distance of ten layers of the Au crystallites is determined as 2.35 nm (or 0.235 nm per lattice space), corresponding to the (1 1 1) crystallographic planes of cubic Au (JCPDS 04-0784). The morphology of P3HT/Pt was also obtained by TEM and shown in Figure 2(c). The P3HT with chain structure curled like irregular rings. The size of Pt nanoparticles is 3~5 nm as shown in the inset in Figure 2(c). The distance of 10 layers of lattice spaces of Pt crystallite are determined as 2.26 nm (or 0.226 nm per interplanar spacing, inset in Figure 2(c)), which match the (1 1 1) crystallographic plane of Pt (JCPDS 04-0802). These results indicated that the two metal-polymer semiconductor heterojunction structures (g-C_3N_4/Au and P3HT/Pt) indeed formed. Figure 2(d) shows the TEM images of g-C_3N_4/Au/P3HT/Pt. The unobvious image contrast between g-C_3N_4 and P3HT may lead us not to distinguish the two polymer semiconductors under the TEM or even under the HRTEM. Therefore, it is difficult to confirm the Au-P3HT heterostructure in g-C_3N_4/Au/P3HT/Pt by using TEM.

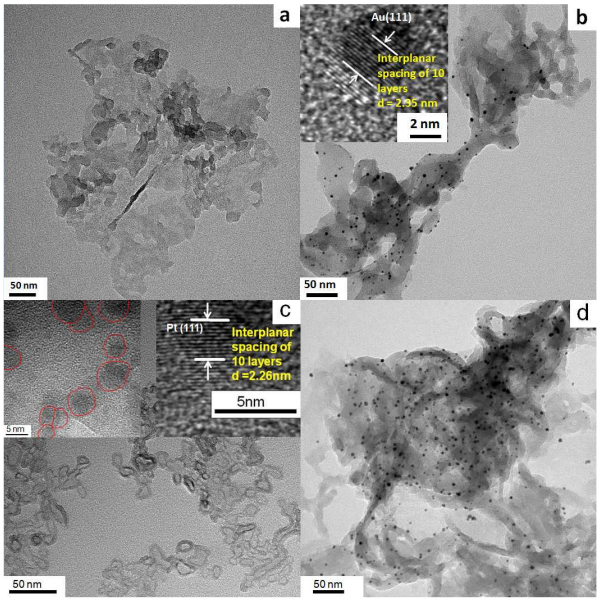

Figure 2 TEM images of (a) g-C_3N_4, (b) g-C_3N_4 /Au, (c) P3HT/Pt, and (d) g-C_3N_4/Au/P3HT/Pt obtained by the self-assembly method. The inset in b shows the HRTEM image of Au nanoparticles. The left insert in c shows the TEM image of Pt nanopartilcles loaded on P3HT. The right insert in c shows the HRTEM of Pt nanoparticles.

To confirm the formation of Au-P3HT heterostructure in g-C_3N_4/Au/P3HT/Pt, XPS was applied for elemental analysis and valence state analysis of the samples. As expected, in the sample of g-C_3N_4/Au/P3HT/Pt, the peak at binding energy of 163.85 eV for S 2p was observed (see in Figure 3 (a)). The observed sulfur signal suggested that P3HT exists in the sample of g-C_3N_4/Au/P3HT/Pt because only the P3HT contains S element in the component parts of heterostructure. The high-resolution Au 4f XPS spectra of g-C_3N_4/Au and g-C_3N_4/Au/P3HT/Pt are shown in Figure 3 (b). The Au 4f spectra consist of two peaks due to the electron spin. The binding energy of Au 4f 5/2 and Au 4f 7/2 for g-C_3N_4/Au was found at around 83.26 and 86.94 eV, respectively. However, the binding energy of Au 4f 5/2 and Au 4f 7/2 for g-C_3N_4/Au/P3HT/Pt was found at around 83.35 and 87.03 eV, respectively. There is about 0.09 eV shift towards high binding energy. This shift indicated the chemical state of Au loaded on the g-C_3N_4 changed after mixed g-C_3N_4/Au with P3HT/Pt. In consideration of the results of XPS, the experimental method and the Au-S bond formed between S element in the organics and Au, [32, 33] we speculated that P3HT/Pt was successfully integrated with g-C_3N_4/Au and this combination was due to the formation of Au-S bond between Au on the g-C_3N_4 and S in the P3HT. It is the formation of Au-S bond led the Au 4f spectra of g-C_3N_4/Au/P3HT/Pt to shift towards high binding energy.

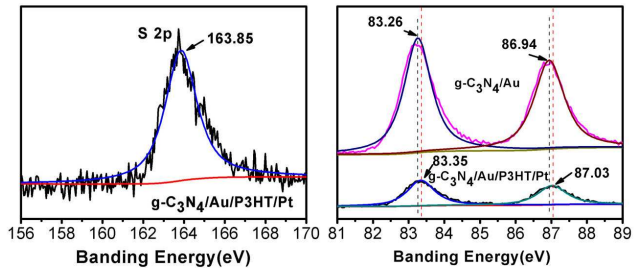

Figure 3 The high-resolution XPS spectra of (a) S 2p for the g-C_3N_4/Au/P3HT/Pt and (b) Au 4f for the g-C_3N_4/Au and g-C_3N_4/Au/P3HT/Pt.

Optical properties of g-C_3N_4/Au/P3HT/Pt

The UV-visible diffuse reflectance spectra of g-C_3N_4, g-C_3N_4/Au, g-C_3N_4/Au/P3HT/Pt are shown in Figure 4. The strong absorption band of all these photocatalysts are shorter than 400 nm, implying the less condensation degree of g-C_3N_4. The weak tailed absorption band at 400~700 nm observed in g-C_3N_4 spectra due to the incorporation of carbon into the melon-based carbon nitride structures.[12] The absorption intensity of the g-C_3N_4/Au and g-C_3N_4/Au/P3HT/Pt photocatalysts increases noticeably in all the detected wave range. The absorption band around 530 nm is due to the surface Plasmon resonance (SPR) of metallic Au nanoparticles.[20,22] For the sample of g-C_3N_4/Au/P3HT/Pt, the intensity of the absorption band around 530 nm increased further, indicating that combining g-C_3N_4/Au with P3HT/Pt enhanced the SPR effect of Au particles. These results further confirm the formation of conjunction between P3HT and Au.

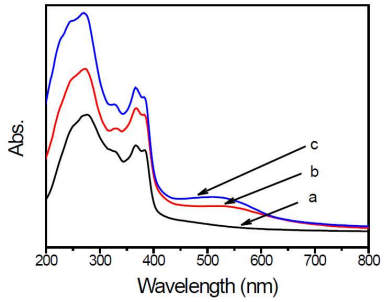

Figure 4 UV-Vis diffuse reflectance spectra (DRS) of (a) g-C_3N_4, (b) g-C_3N_4/Au, and (c) g-C_3N_4/Au/P3HT/Pt.

The PL spectra analysis was used to study the transfer and recombination processes of photogenerated electron-hole pairs in photocatalysts. Figure 5 shows the PL spectra of pure g-C_3N_4, g-C_3N_4/Au and g-C_3N_4/Au /P3HT/Pt under incident light with a wavelength of 279 nm. All PL spectra of the samples have the same major peak at 457 nm, which could be attributed to the recombination of photoexcited electron-hole in g-C_3N_4 with a band gap at 2.7 eV. Significant PL quenching was observed in g-C_3N_4/Au and g-C_3N_4/Au/P3HT/Pt. The quenching of g-C_3N_4/Au could be contributed to the electrons migration from g-C_3N_4 to the Au particles, which was more conducive to the photoreduction of H^+ to H_2. Compared to g-C_3N_4, nearly 75% PL quenching was observed in the sample of g-C_3N_4/Au/P3HT/Pt, indicating that the g-C_3N_4/Au/P3HT/Pt photocatalyst has a lower recombination of the photogenerated electron-hole pairs and more efficiently charge transfer between g-C_3N_4 and P3HT due to the tightly conjunction between them.

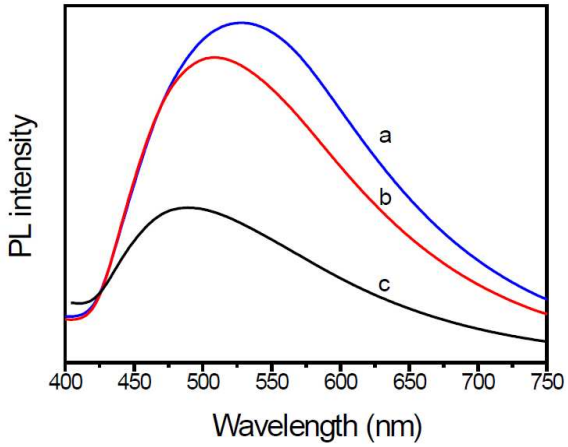

Figure 5 Photoluminescence (PL) emission spectra of (a) g-C_3N_4 , (b) Au loaded g-C_3N_4, and (c) g-C_3N_4/Au/P3HT/Pt heterostructure. The excited wavelength was 279 nm.

Photocatalytic activity and photocatalytic mechanism

Photocatalytic H_2 production were evaluated under visible light irradiation ($\lambda > 420$ nm) using TEA as sacrificial reagent. Figure 6 shows the H_2 evolution rate on different g-C_3N_4-based photocatalysts. As shown in the figure 6, the photocatalyst of g-C_3N_4/P3HT shows a negligible H_2 evolution rate. However, after loading of Pt on P3HT, the H_2 evolution rate of g-C_3N_4/P3HT/Pt reaches at 74 μmol h^{-1}. This enhanced photocatalytic H_2 evolution rate could be ascribed to the efficiently separation of the photo generated electron-hole pairs in g-C_3N_4/P3HT/Pt photcatalyst and the platinum on the P3HT act as an electron outlet or active site for the reduction of H^+. The photocatalytic H_2 evolution rate on g-C_3N_4/Au and g-C_3N_4/Pt is 73 μmol h^{-1} and 82 μmol h^{-1}, respectively. Loaded both Au and Pt on g-C_3N_4 can enhance the photocatalytic performance further. The photocatalytic H_2 evolution rate on g-C_3N_4/Au-Pt is 171μmol h^{-1}, approximating to the sum of H_2 evolution rate on g-C_3N_4/Au and g-C_3N_4/Pt. These results also indicated that Au on the g-C_3N_4 played a similar role as Pt as the electron outlet or active site. It is well known that the more electrons on the active site of Au surface (ex. g-C_3N_4/Au) or the active site of Pt surface (ex. g-C_3N_4/Pt or g-C_3N_4/Au/P3HT/Pt), the more conducive to the H_2 generation. Comparing to the H_2 evolution rate of g-C_3N_4/Au, the H_2 evolution rate of g-C_3N_4/Au/P3HT decreased from 73 μmol h^{-1} to 56 μmol h^{-1}. This indicated that after the combination of P3HT on the g-C_3N_4/Au, the Au suface did not gain more effective electrons for H_2 evolution and the excited P3HT would not supply the electrons to the Au suface directly for H_2 evolution or transfer excited electons to g-C_3N_4 then to Au surface for H_2 evolution. The result reflected the fact that the combination of P3HT led the electrons on the Au surface to be efficiently consumed, which indicated that P3HT "grabbed" the electrons on the Au surface through the way that providing holes to Au surface. The H_2 evolution rate of g-C_3N_4/Au/P3HT/Pt is 320 μmol h^{-1}, more than four times higher than that of g-C_3N_4/P3HT/Pt, g-C_3N_4/Au or g-C_3N_4/Pt, respectively. It is worth noting that the photocatalytic H_2 evolution rate of g-C_3N_4/Au/P3HT/Pt is more than 2 times higher than that of g-C_3N_4/Au-Pt. In this case, the P3HT can be compared to an "electric wire" which transferred the elections to the far end (the realization of separating electron-hole pairs) where Pt used them for the H_2 generation. These results indicate that in the heterostructure of g-C3N4/Au/P3HT/Pt, the combination of electrons on the Au surface with the holes from the HOMO of P3HT was favourable to preventing the recombination of electron-hole pairs in their body of g-C_3N_4 and P3HT. Therefore, the Pt could obtain more electrons for H_2 evolution and the g-C_3N_4 could reserve more holes for the oxidation of TEA.

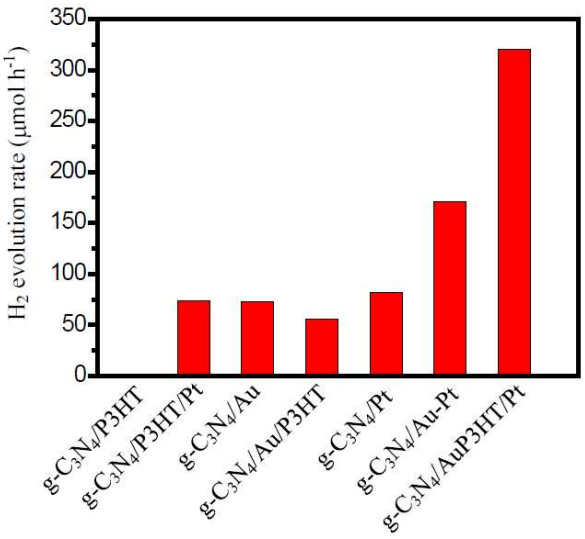

Figure 6 The H_2 evolution rates of various photocatalysts. All the experimental data were obtained under identical reaction conditions. The light source was 300W Xe lamp (λ>420nm) and TEA (10% in volume) was chosen as the sacrificial reagent.

Figure 7 shows the H_2 evolution rate on g-C_3N_4/Au/P3HT/Pt with different amount of P3HT. As shown in Figure 7, with the increase of the amount of P3HT, the photocatalytic H_2 evolution rate increases first and reaches a maximum of 320 μmol h^{-1} when the amount of P3HT is about 0.5 wt %. However, further increasing the amount of P3HT leads to decrease of the photocatalytic H_2 evolution.

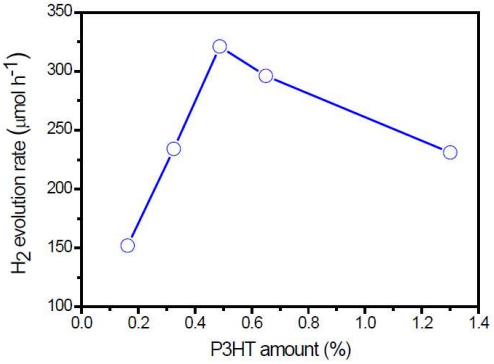

Figure 7 The rate of H_2 evolution on g-C_3N_4/Au/P3HT/Pt polymer composites with different amounts of P3HT under visible light (λ> 420 nm).

The mechanism of photocatalysts is shown in the Scheme 1. Here we apply the metal- semiconductor contact theory and the Fermi level equilibration principle involving the Schottky–Mott limit demonstrated by Tang and Slyke [34] and the Metal-organic interface proposed by Antonie Kahn, Norbert Koch and Weiyang Gao[35] to explain the photocatalysis mechanism of the g-C_3N_4/Au/P3HT/Pt. The Charge distribution leads to Fermi level equilibration in the metal-semiconductor system, so we can assume a quasi-fermi level (E_F*) in the g-C_3N_4/Au/P3HT/Pt. The property to store of electrons in a quantized fashion in Au nanoparticles [36, 37] leads to the shift of Fermi level of Au towards more negative potential. This may result in the Fermi level of the composite shifts closer to the conduction band of semiconductor in the ZnO/Au systems or TiO_2/Au system.[38, 39] In the g-C_3N_4/Au system, the upward shift of the Fermi level (E_F) of the composite to the quasi-Fermi level (E_F*) in Scheme 1 have been used for reference and the photocatalytic performance of g-C_3N_4 improved due to the efficiency of interfacial charge-transfer process.[20]

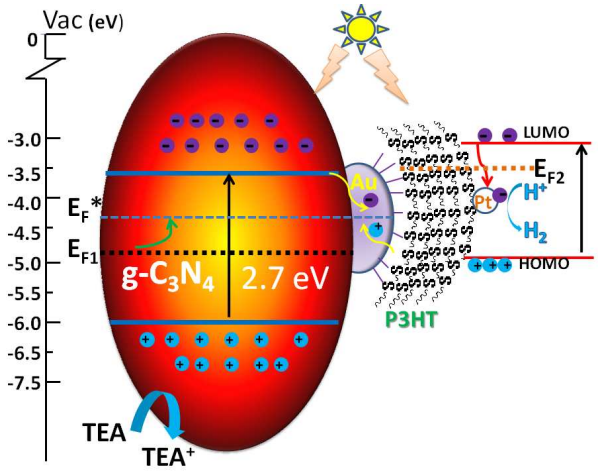

Scheme 1 The Scheme for the photocatalytic mechanism of g-C_3N_4/Au/P3HT/Pt heterostructure

On the other hand, the high work function of Au leads to small hole injection barriers (HIBs) at the metal/organic interface and it often was chosen as electrode for hole injection.[40] The HIB is defined as the energy difference between the metal Fermi level (E_F) and the hole transport level in the organic semiconductor. In this scheme, the highest occupied molecular orbital (HOMO) can be regard as the hole transport level in P3HT. However, contaminated Au surface work function values spanned the range between 4.7–5.1 eV and may even be larger when considering different environment.[41] The HOMO of P3HT(π-conjugated polymer) was determined at 5.1 eV or 4.9 eV (bulk [42,43]), 4.3 eV (film[44]), 4.0 eV (a single strand[45]). If we neglect the effect of interface dipoles (IDs), admitting that the Au-S bond indeed formed between Au and P3HT, the values of Au surface work function and the HOMO of P3HT were so close that the HIBs of the interface between the P3HT and Au was very low and even form an ohmic contact.[46] The low potential barrier or ohmic contact of P3HT/Au favors the charge carrier inject into each other. The holes, which transport through the P3HT network (good hole-transport materials),[47] will be collected at the Au surface.

In our research, however, the formation of Au-S bond was confirmed by XPS. Therefore, the energy level alignment in reactive interfaces is controlled by chemistry-induced electronic states.[37] The chemical reaction to form Au-S bond leads to the formation of gap states and pinning of E_F at the interface. Just consider the interface of P3HT/Au, if the Au work function falls in the P3HT gap, the gap states pinning E_{F2} lies in the upper part of the gap and rise the hole injection barrier,[48] while the contaminated Au has a more larger work function, and the large surface dipole (SD) of Au work function also leads to the large interface dipole barrier.[35] The large HIBs results in low hole transfer and compresses the photocatalytic efficiency. The HIBs of P3HT/Au was determined at 0.59 eV [49] or even smaller at 0.35eV,[40] because of the different preparative approaches or the presence of ambient contamination at the Au interfaces.[41]

Naturally, the interface charge-transfer of g-C_3N_4/Au and the chemical bond of P3HT/Au or other unforeseen mechanism, like molecule-induced modification of the metal work function, contribute to the IDs and affect each other. This becomes more complex and difficult to differentiate between the various contributions. [35]

In our experiment, by comparing the rate of photocatalytic H_2 evolution on g-C_3N_4/Au and g-C_3N_4/Au/P3HT, it is concluded that the effective electrons on the Au suface were consumed and that the P3HT "grabbed" the electrons on the Au surface through the way that providing holes to Au surface. This means the interface of P3HT/Au realized the hole transport from P3HT to the Au surface. This let us suspected a low potential barrier had been formed at the P3HT/Au interface for the injection of charge carrier into each other. The recombination of electrons generated in the g-C_3N_4 with the holes from the HOMO level of P3HT on the Au nanoparticles surface promoted the efficient dissociation of electron-hole pairs generated in the two kind of polymer semiconductors. The excited electrons in the P3HT transfered to the Pt and achieved the reduction of H^+ to H_2. The g-C_3N_4 got the compensation of electrons through the oxidation of TEA to TEA^+. The recombination process of electrons and holes on the Au surface and the dissociation process of photo-generated electron-hole pairs in the g-C_3N_4 and P3HT greatly enhanced the overall photocatalytic efficiency. The Platinum metal introduced an ohmic contact that provided a quick transfer of electrons to the electrolyte.[38] This resulted in the Fermi energy of Pt remained close to the solution redox level and had a negligible effect on the Fermi level of the semiconductor.

Conclusions

In summary, the tightly coupled heterostructure g-C_3N_4/Au/P3HT/Pt was successfully prepared. Au and Pt nanoparticles with size of 3~5 nm were uniformly loaded on g-C_3N_4 and P3HT, respectively. The XPS result indicates the formation of Au-S bond in g-C_3N_4/Au/P3HT/Pt photocatalyst. The remarkably PL quenching of g-C_3N_4/Au/P3HT/Pt photocatalyst indicates a lower recombination of the photogenerated electron-hole pairs. The as-prepared heterojunction g-C_3N_4/Au/P3HT/Pt promoted the transfer of light-excited electrons from g-C_3N_4 to the P3HT effectively and enhanced photocatalytic hydrogen production under visible light. The g-C_3N_4/Au/P3HT/Pt with amount P3HT at 0.5wt% achieves the highest H_2 evolution rate and the photcatalytic H_2 evolution rate reaches 320 μmol h^{-1}.

Acknowledgements

We thank the National Natural Science Foundation of China (No. 21273157) for the financial support. We thank Sichuan University Analytical & Testing Centre for the analysis of PL and XRD, and especially to Dr S. L. Wang and Dr G. P. Yuan for TEM measurements.

Notes and references

[a] *College of Materials Science and Engineering, Sichuan University, 610064, P. R.China. Fax: +86-28-85416050; Tel: +86-28-85412415; E-mail: nic0402@scu.edu.cn*

[b] *College of Chemistry, Sichuan University, Chengdu, 610064, P. R. China. Fax: 86 2885221339; Tel: 86 13551341892; E-mail: hjyan@scu.edu.cn*

1 P. P. Edwards, V. L. Kuznetsov, W. I. F. David, *Phil. Trans. R. Soc. A* 2007, **365**, 1043.
2 J. A. Turner, *Science* 2004,**305**, 972.
3 A. Fujishima, K. Honda, *Nature* 1972, **238**:37.
4 K. Maeda, X. C. Wang, Y. Nishihara, D. L. Lu, M. Antonietti, K. Domen, *J. Phys. Chem. C* 2009, **113**: 4940.
5 K. Maeda, K. Domen, *J. Phys. Chem. C* 2007, **111**:7851.
6 X. C. Wang, K. Maeda, A. Thomas, K. Takanabe, G. Xin, J. M. Carlsson, K. Domen, M. Antonietti, *Nature metar.* 2009, **8**: 76.
7 J. S. Zhang, J. H. Sun, K. Maeda, K. Domen, P. Liu, M. Antonietti, X. Z. Fu, X. C. Wang, *Energy Environ. Sci.*, 2011, **4**: 675.
8 X. C. Wang, K. Maeda, X. F. Chen, K. Takanabe, K. Domen, Y. D. Hou, X. Z. Fu, M. Antonietti, *J. Am. Chem. Soc.* 2009, **131**: 1680.
9 J. H. Liu, T. K. Zhang, Z. C. Wang, G. Dawson, W. Chen, *J. Mater. Chem.* 2011, **21**: 14398.
10 T. Tyborski, C. Merschjann, S. Orthmann, F. Yang, M-Ch Lux-Steiner, Th Schedel-Niedrig, *J. Phys.: Conden. Matter*, 2012, **24**: 162201.
11 H. J. Yan, Y. Chen, S. M. Xu, *Int. J. Hydrogen Energ*. 2012, **37**: 125.
12 H. J. Yan, *Chem. Commun*. 2012, **48**: 3430.
13 G. Xin, Y. L. Meng, *J. Chem.* 2013, 187912.
14 Y. Ham, K. Maeda, D. Cha, K. Takanabe, K. Domen, *Chem. Asian J.* 2013, **8**: 218.
15 S. Martha, A. Nashim, K. M. Parida, *J. Mater. Chem.* A, 2013, **1**: 7816.
16 G. Liu, P. Niu, C. H. Sun, S. C. Smith, Z. G. Chen, G. Q. Lu, H. M. Cheng, *J. Am. Chem. Soc.* 2010, **132**: 11642.
17 B. Yue, Q. Y. Li, H. Iwai, T. Kako, J. H. Ye, *Sci. Technol. Adv. Mater.* 2011, **12**: 034401.
18 K. Takanabe, K. Kamata, X. C. Wang, M. Antonietti, J. Kubota, K. Domen, *Phys. Chem. Chem. Phys.* 2010, **12**: 13020.
19 S. X. Min, G. X. Lu, *J . Phys. Chem. C*, 2012, **116**: 19644.
20 D. Yan, X. C. Wang, A. Thomas, M. Antonietti, *Chem. Cat. Chem*. 2010, **2**:834.
21 J. H. Liu, Y. W. Zhang, L. H. Lu, G. Wu, W. Chen, *Chem. Commun*. 2012, **48**: 8826.
22 S. Samanta, S. Martha, K. Parida, *Chem. Cat. Chem*. 2014, **6**: 1453
23 M. Bledowski, L. Wang, A. Ramakrishnan, O. Khavryuchenko, V. Khavryuchenko, P. Ricci, J. Strunk, T. Cremer, C. Kolbeck, R. Beranek, *Phys. Chem. Chem. Phys.* 2011, **13**:21511.
24 D. Mitoraj, R. Beranek, H. Kisch, *Photochem. Photobiol. Sci.* 2010, **9**: 31.
25 X. X. Xu, G. Liu, C. Randorn, J. T. S. Irvine, *Int. J. Hydrogen Energy* 2011, **36**: 13501.
26 H. W. Kang, S. N. Lim, D. S. Song, S. B. Park, *Int. J. Hydrogen Energy* 2012, **37**: 11602.
27 F. Yang, M. Lublow, S. Orthmann, C. Merschjann, T. Tyborski, M. Rusu, S. Kubala, A. Thomas, R. Arrigo, M. Hävecker，M. Schedel-Niedrig, *ChemSusChem* 2012, **5**: 1227.
28 L. Ge, C. C. Han, *Appl. Catal. B: Environ.* 2012, **117**: 268.
29 H. J. Yan, Y. Huang, *Chem. Commun.* 2011, **47**: 4168.
30 J. S. Zhang, M. W. Zhang, R. Q. Sun, X. C. Wang, *Angew. Chem. Int. Ed.* 2012, **51**: 10145.
31 S. C. Yan, Z. S. Li, Z. G. Zou, *Langmuir* 2009, **25**:10397.
32 L. J. Wang, G. M. Rangger, Z. Y. Ma, Q. K. Li, Z. G. Shuai, E. Zojer, G. Heimel, *Phys. Chem. Chem. Phys*. 2010, **12**: 4287.
33 F. Tielens, E. Santos, *J. Phys. Chem. C* 2010, **114**: 9444.
34 C. W. Tang, S. A. Slyke, *App.l Phys. Lett.* 1987, **51**: 913.
35 A. Kahn, N. Koch, W. Y. Gao, *J. Polym. Sci. Part B* 2003, **41**: 2529.
36 S. W. Chen, R. W. Murray, *J. Phys. Chem. B* 1999, **103**: 9996.
37 S. Chen, R. S. Ingram, M. J. Hostetler, J. J. Pietron, R. W. Murray, T. G. Schaaff, J. T. Khoury, M. M. Alvarez, R. L. Whetten, *Science* 1998, **280**: 2098.
38 A. Wood, M. Giersig, P. Mulvaney, *J. Phys. Chem. B* 2001, **105**: 8810.
39 V. Subramanian, E. E. Wolf, P. V. Kamat, *J. Am. Chem. Soc* 2004, **126**: 4943.
40 S. Rentenberger, A. Vollmer, E. Zojer, R. Schennach, N. Koch, *J. Appl. Phys.* 2006, **100**: 053701.
41 A. Wan, J. Hwang, F. Amy, A. Kahn, *Org. Electron*. 2005, **6**: 47.
42 M. C. Scharber, D. Mühlbacher, M. Koppe, P. Denk, C. Waldauf, A. J. Heeger, C. J. Brabec, *Adv. Mater*. 2006, **18**: 789.
43 V. Shrotriya, G. Li, Y. Yao, C. W. Chu, Y. Yang, *Appl. Phys. Lett.* 2006, **88**: 073508.
44 R. P. Mikalo, D. Schmeißer, *Synth. Met.* 2002, **127**: 273.
45 Y. Kanai, J. C. Grossman, *Nano Lett.* 2008, **8**:908
46 C. H. Lei, A. Dasa, M. Elliott, J. E. Macdonald, M. L. Turner, *Synthetic Met.* 2004, **145** : 217
47 Wendy U. Huynh, Janke J. Dittmer, A. Paul Alivisatos. *Science* **295**, 2425 (2002);
48 Y. D. Park, J. H. Cho, D. H. Kim, Y. S. Jang, H. S. Lee, K. W. Ihm, T. H. Kang, K. W. Cho, *Electrochem. Solid ST* 2006, **9**: G317-G319.
49 J. E. Lyon, A. J. Cascio, M. M. Beerbom, R. Schlaf, Y. Zhu, S. A. Jenekhe, *Appl. Phys. Lett.* 2006, **88**: 222109.

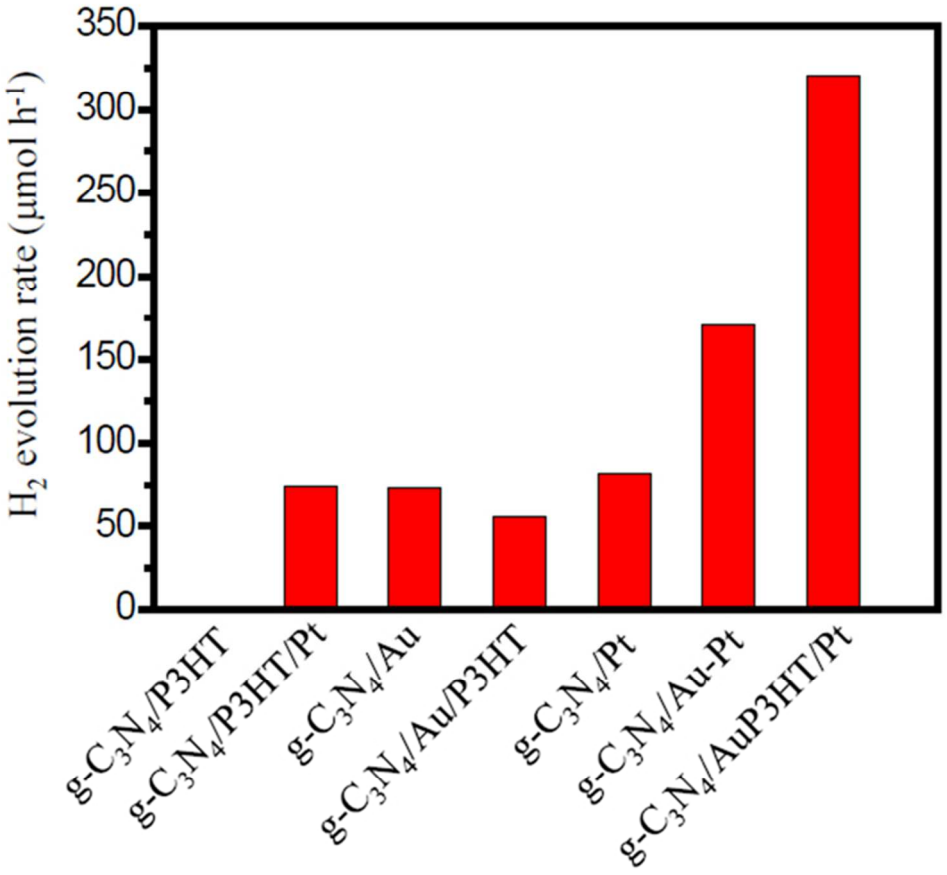

235x207mm (72 x 72 DPI)